

Nonclassical imaging via photon-number fluctuation correlation

Jane N. Sprigg, Tao Peng, Yanhua Shih

Department of Physics, University of Maryland Baltimore County, Baltimore, MD 21250, USA

We report an experimental study on a nonclassical imaging mechanism. By achieving a convolution between the aperture function of the object and the photon-number fluctuation correlation function of thermal light, we isolated a well-resolved image from the unresolved classical image as well as the autocorrelation of two identical unresolved classical images. The remarkable feature of this mechanism is that its imaging resolution depends on the angular size of the light source instead of that of the imaging lens.

The imaging resolution of a classical camera is limited by the size of its lens, D , and the distance to the object, s_o . Mathematically, a classical image is the result of the following convolution:

$$\begin{aligned} I(\vec{\rho}_i) &= \int d\vec{\rho}_o A^2(\vec{\rho}_o) \text{somb}^2 \frac{\pi D}{\lambda s_o} (|\vec{\rho}_o - \vec{\rho}_i/\mu|) \\ &\equiv A^2(\vec{\rho}_o) \otimes \text{somb}^2 \frac{\pi D}{\lambda s_o} (|\vec{\rho}_o - \vec{\rho}_i/\mu|) \end{aligned} \quad (1)$$

where $I(\vec{\rho}_i)$ is the intensity distribution on the image plane; $\vec{\rho}_o$ and $\vec{\rho}_i$ are the transverse coordinates of the object-plane and the image-plane, respectively; $A(\vec{\rho}_o)$ is the aperture function of the object; the sombrero-like function, or Airy disk, $\text{somb}(x) = 2J_1(x)/x$ is the so-called image-forming function, where $J_1(x)$ is the first-order Bessel function. Inside the somb-function, λ is the wavelength of the illumination and $\mu = -s_i/s_o$ is the image magnification. For large values of D/s_o , the somb-function can be approximated as a δ -function of $|\vec{\rho}_o - \vec{\rho}_i/\mu|$, which results in perfect point-to-point imaging, i.e., light from an object point $\vec{\rho}_o$ stops at a unique point $\vec{\rho}_i$ on the image plane. However, when D/s_o is not large enough, it requires a greater value of $|\vec{\rho}_o - \vec{\rho}_i/\mu|$ for the somb-function, or the Airy disk, to reach its zero, which results in a point-to-spot imaging function, i.e., light from an object point stops at a unique “spot” on the image plane. Obviously, the size of the spot determines the “resolution” of the convolution and thus the imaging resolution of the camera. We usually use Rayleigh’s criterion to define the resolution of an optical imaging device [1]. For long-distance imaging, a camera needs to have a large enough imaging lens to achieve a certain expected resolution. Otherwise, the picture will be “blurred” even if the camera has enough “zooming” power for that distance. For example, working in visible wavelengths, a classical camera needs a lens of $D = 90$ m in order to distinguish two points with $200 \mu\text{m}$ separation at $s_o = 10$ km distance.

Why does a smaller imaging lens lose its ability to distinguish two close points on the object plane? Although light-rays coming from an object point $\vec{\rho}_o$ may propagate with different directions and thus with different optical paths, a lens forces all of them to travel equal distances to arrive at a unique point $\vec{\rho}_i$ on the image plane, re-

sulting in constructive interference at that unique image point. Simultaneously, the lens introduces phase delays between these optical paths which are large enough to result in destructive interference for $\vec{\rho}'_i \neq \vec{\rho}_i$, and causes light-rays from a neighboring object-point $\vec{\rho}'_o$ to interfere destructively at $\vec{\rho}_i$. However, a smaller lens may not be able to introduce large enough phase delays among these rays, resulting in incomplete destructive interference. It is this incomplete destructive interference which produces point-to-spot imaging, or partially overlapped images between two neighboring object points, and limits the resolution of an image. We thus consider classical imaging the result of the first-order coherence of light, with an imaging resolution limited by the size of the imaging lens or other mechanisms that limit the ability to achieve complete first-order constructive-destructive interferences. It is interesting that the image is produced by constructive interference but its resolution is limited by the destructive interference.

One solution to surpass the Rayleigh resolution limit is to measure the higher-order intensity correlation of light rather than the intensity. A recent experiment by Oh et. al. [2] successfully demonstrated a $\sim\sqrt{2}$ gain in imaging resolution from the product of two identical classical images via “speckle illumination.” We may roughly divide these higher-order imaging mechanisms into two groups: (1) the imaging resolution is determined by the first-order coherence of light; (2) the imaging resolution is determined by the second-order coherence of light. The experimental demonstration of Oh et. al. belongs to group (1) [3].

In fact, as we will discuss in this Letter, using a similar setup to that of Oh et. al. the imaging resolution can be improved significantly if we change the image-forming mechanism from group one to group two by achieving the following convolution[4] between the object aperture function and the photon-number fluctuation correlation, $\langle \Delta n_1 \Delta n_2 \rangle$:

$$\begin{aligned} R_c(\vec{\rho}_1) &\propto A^2(\vec{\rho}_2/\mu) \otimes \langle \Delta n_1 \Delta n_2 \rangle \\ &= A^2(\vec{\rho}_2/\mu) \otimes \text{somb}^2 \left(\frac{\pi \Delta \theta_s}{\lambda} |\vec{\rho}_1 - \vec{\rho}_2|/\mu \right) \end{aligned} \quad (2)$$

where $\vec{\rho}_1$ is the transverse coordinate of the scanning detector D_1 , or the CCD element, and $\vec{\rho}_2$ is the transverse

coordinate of the bucket detector D_2 that is integrated as the convolution parameter; $\Delta\theta$ is the angular diameter of the thermal light source; μ is the magnification factor of the imaging lens. Comparing this with the classical imaging resolution in Eq. 1, we find Eq. 2 gives a nonclassical resolution that is determined by the angular diameter of the thermal light source. If the angular size of the light source is large enough, a well-resolved image is observable in the convolution coincidences even if the classical image as well as its higher-order products are completely “blurred” out due to the “smaller” lens; the experiment reported in this Letter confirms Eq. 2.

In addition to its nonclassical imaging resolution, the photon-number fluctuation correlation $\langle \Delta n_1 \Delta n_2 \rangle = \text{somb}^2(\pi\Delta\theta/\lambda)(|\vec{\rho}_1 - \vec{\rho}_2|/\mu)$ is also “turbulence-free” [5, 6]. These aspects are particularly attractive for sunlight long-distance imaging: the angular diameter of the sun is $\sim 0.53^\circ$, providing in principle a turbulence-free resolution of $200 \mu\text{m}$ for any object on earth at any distance without the need of huge lenses.

A diagram of the experimental setup is shown in Fig. 1. Although the imaging working principle is similar to that of the original lensless “ghost imaging” experiment [7], the object of this setup is directly viewed by both the bucket detector and the CCD, in contrast to a “ghost imaging” setup in which the object is only viewed by the bucket detector while the CCD directly faces the light source.

The optical part of the setup is similar to the experiment of Oh et. al. [2], with the addition of a “bucket” detector and a positive-negative fluctuation correlation circuit (PNFC) [8–10]. The use of the “bucket” detector and the PNFC circuit results in a completely different image-forming mechanism from that of [2].

With the setup outlined in Fig. 1, we can simultaneously measure three different types of image: a classical image; the product of two identical classical images; and the convolution between the object aperture function and the photon-number fluctuation correlation function as shown in Eq. 2. We thus are able to directly compare the imaging resolution for these three different imaging mechanisms.

The object was a standard resolution testing gauge 1951 USAF. The portion of the object used in the measurement was the 5-3 element of the resolution gauge, which has three slits with a width and separation of $12.41 \mu\text{m}$. The transverse size of the pseudo-thermal source was approximately 6 mm in diameter, resulting in an $8.7 \mu\text{m}$ resolution on the object plane which is enough to resolve the slits. A pinhole placed after the imaging lens simulated various lens diameters; for a pinhole diameter of 1.5 mm, the smallest feature that can be resolved in the object plane is $\delta x \simeq 35 \mu\text{m}$ which is not enough to resolve the slits.

Typical experimental results are presented in Fig. 2. Figure 2a shows a completely unresolved first order clas-

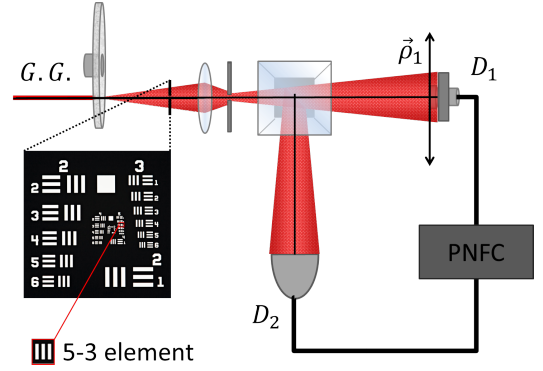


FIG. 1. Schematic of the experiment. The optical part is similar to that of [2], with the addition of a “bucket” detector. This experiment uses a typical pseudo-thermal light source, which consists of a He-Ne laser beam and a rotating ground glass. The ground glass (G.G.) scatters the 6 mm laser beam into pseudo-thermal light. The pseudo-thermal light, starting from plane $z = 0$, illuminates an imaging resolution gauge (1951 USAF) at plane $z = z_o$ and then passes through an imaging lens at $z = z_o + s_o$. An adjustable aperture behind the lens simulates different lens diameters. A beamsplitter is placed after the lens to guide the field to photodetectors D_1 and D_2 . D_1 is a point-like detector that can be scanned on the image plane of $z = z_o + s_o + s_i$. The bucket detector D_2 is also placed in the image plane, on the opposite side of the beamsplitter. The PNFC circuit measures the photon-number fluctuation correlation between D_1 and D_2 and images the object with a magnification of μ in the fluctuation correlation.

sical image of the three slits that was directly measured by the scanning detector. Fig. 2b shows two results: the black dots plot the product of two unresolved classical images, which was calculated by squaring the first-order intensity $[n_1(\vec{\rho}_1)]^2$ at each scanning point, while the red circles show the product of the fluctuations $[\Delta n_1(\vec{\rho}_1)]^2$ at each point. This fluctuation autocorrelation was calculated from the photon-number counting of D_1 , similar to the measurement performed in [2]. This method produces a $\sqrt{2}$ resolution gain $\delta x/\sqrt{2} = 25 \mu\text{m}$ which, as seen in 2b, is still not enough to resolve the three slits. However, by taking advantage of our imaging method based on the convolution measurement of Eq. 2, a well-resolved image of the 5-3 element of the gauge was observed as shown in Fig. 2c.

The error bars for the unresolved classical image are much smaller than those of Fig. 2c for the following reasons: (1) The statistics of the unresolved classical image is that of a first-order measurement, while the statistics of Fig. 2c is that of a second-order measurement: the single-detector counting rate is much higher than the coincidence counting rate. (2) The photon-number fluctuation calculation introduced additional error due to the low count ($\bar{n} \sim 8/\text{time window}$). This could easily be reduced by recording more counts per time window. In

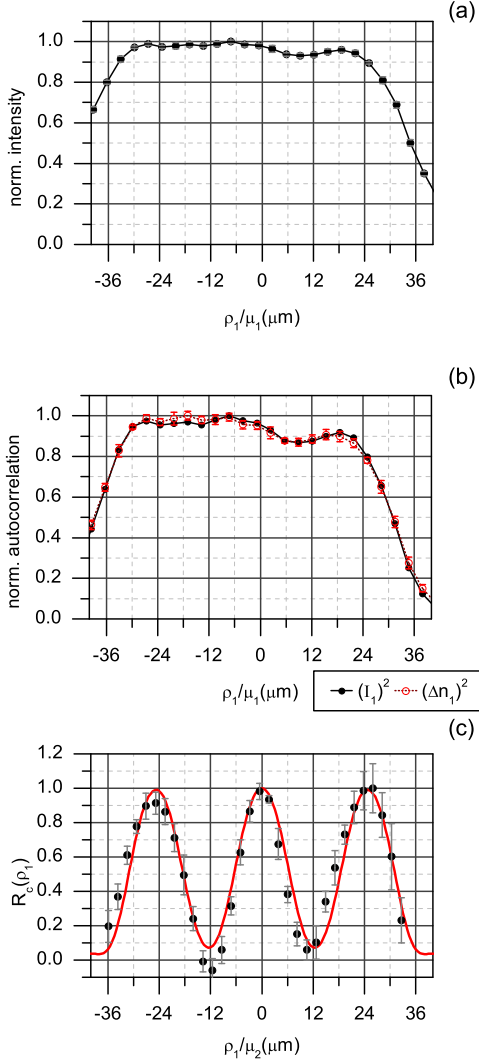


FIG. 2. Resolution comparison in the object plane for different imaging technologies of three $12.41 \mu\text{m}$ wide slits imaged by a 6 mm diameter source: (a) unresolved classical first-order image; (b) unresolved images from the product of two identical classical images (speckle-to-speckle autocorrelation). The red dots are the result of speckle fluctuation, as seen in [2], the black dots indicate the intensity squared image; (c) completely resolved image observed from the convolution measurement. The black dots are the experimental data, the solid red curve is a theoretical fitting in the object plane of Eq. 2.

general, in order to achieve the same level of statistics as a first-order measurement, a second-order measurement must be recorded for a longer time or at a higher intensity. This appears to be the price to pay for achieving a resolved second-order image in similar light conditions.

In addition to the imaging resolution comparison, we have also studied the imaging resolution of this setup with different sizes of the pseudo-thermal light source. We found its resolution is indeed dependent on the an-

gular diameter of the source as expected from Eq. 2.

In the following, we give a simplified analysis of the experimental observation. We assume an experimental condition in which the first-order classical images are all “blurred” out due to the small size of the lens, as is the case in our experiment. Under this condition we examine the photon-number fluctuation correlation $\langle \Delta n_1 \Delta n_2 \rangle$. If $\langle \Delta n_1 \Delta n_2 \rangle$ is still able to resolve the aperture function, then the convolution between the aperture function and $\langle \Delta n_1 \Delta n_2 \rangle$ is still able to produce a resolvable image.

We describe the thermal source as a large number of independent and randomly radiated point sub-sources evenly distributed on a disk normal to the object plane. In a natural thermal source, such as the sun, each sub-source corresponds to an atomic transition. In our pseudo-thermal source, millions of tiny scattering diffusers on the rotating ground glass play the role of sub-sources. The diffusers scatter the laser beam to all possible directions denoted by \mathbf{k} , during which the scattered fields also acquire random phases. $|\alpha_m(\mathbf{k})\rangle$ describes the state of a subfield scattered by the m th diffuser with a vector \mathbf{k} . We assume that the pseudo-thermal field is monochromatic and concentrate on its transverse spatial behavior. We can then write a thermal or pseudo-thermal field in the coherent state representation [11, 12]:

$$|\Psi\rangle = \prod_m |\{\alpha_m\}\rangle = \prod_{m,\mathbf{k}} |\alpha_m(\mathbf{k})\rangle, \quad (3)$$

where m labels the m th subfield that is created or scattered from the m th sub-source and \mathbf{k} is a wavevector. $|\alpha_m(\mathbf{k})\rangle$ is an eigenstate of the annihilation operator with an eigenvalue $\alpha_m(\mathbf{k})$,

$$\hat{a}_m(\mathbf{k})|\alpha_m(\mathbf{k})\rangle = \alpha_m(\mathbf{k})|\alpha_m(\mathbf{k})\rangle. \quad (4)$$

Thus, we have,

$$\hat{a}_m(\mathbf{k})|\Psi\rangle = \alpha_m(\mathbf{k})|\Psi\rangle. \quad (5)$$

The field operator at detector D_j , $j = 1, 2$, can be written in the following form in terms of the sub-sources:

$$\hat{E}^{(+)}(\vec{\rho}_j, t_j) = \int d\mathbf{k} \sum_m \hat{a}_m(\mathbf{k}) g_m(\mathbf{k}; \vec{\rho}_j, t_j) \quad (6)$$

where $g_m(\mathbf{k}; \vec{\rho}_j, t_j)$ is the Green’s function that propagates the m th subfield from the m th sub-source to the j th detector.

Next, we apply the Glauber-Scully theory [11, 13] to calculate the photon-number fluctuation correlation from

the second-order coherence function $G^{(2)}(\vec{\rho}_1, t_1; \vec{\rho}_2, t_2)$:

$$\begin{aligned}
& G^{(2)}(\vec{\rho}_1, t_1; \vec{\rho}_2, t_2) \\
&= \langle \langle \Psi | E^{(-)}(\vec{\rho}_1, t_1) E^{(-)}(\vec{\rho}_2, t_2) E^{(+)}(\vec{\rho}_2, t_2) E^{(+)}(\vec{\rho}_1, t_1) | \Psi \rangle \rangle_{\text{Es}} \\
&= \sum_m \psi_m^*(\vec{\rho}_1, t_1) \psi_m(\vec{\rho}_1, t_1) \sum_n \psi_n^*(\vec{\rho}_2, t_2) \psi_n(\vec{\rho}_2, t_2) \\
&\quad + \sum_{m \neq n} \psi_m^*(\vec{\rho}_1, t_1) \psi_n(\vec{\rho}_1, t_1) \psi_n^*(\vec{\rho}_2, t_2) \psi_m(\vec{\rho}_2, t_2) \\
&= \sum_{m, n} |\psi_m(\vec{\rho}_1, t_1) \psi_n(\vec{\rho}_2, t_2) + \psi_m(\vec{\rho}_2, t_2) \psi_n(\vec{\rho}_1, t_1)|^2 \\
&= \langle n_1 \rangle \langle n_2 \rangle + \langle \Delta n_1 \Delta n_2 \rangle. \tag{7}
\end{aligned}$$

Here $\psi_m(\vec{\rho}_j, t_j)$ is the effective wavefunction of the m th subfield at $(\vec{\rho}_j, t_j)$, which has the following form:

$$\psi_m(\vec{\rho}_j, t_j) = \int d\mathbf{k} \alpha_m(\mathbf{k}) g_m(\mathbf{k}; \vec{\rho}_j, t_j) \tag{8}$$

In the above calculation, we completed the quantum average by considering the commutation rule of the creation and annihilation operators, and the ensemble average by taking into account all possible random relative phases between a large number of incoherent subfields. A detailed calculation can be found in [12].

The photon-number fluctuation correlation is thus:

$$\begin{aligned}
& \langle \Delta n_1 \Delta n_2 \rangle = \\
&= \sum_{m \neq n} \psi_m^*(\vec{\rho}_1, t_1) \psi_n(\vec{\rho}_1, t_1) \psi_n^*(\vec{\rho}_2, t_2) \psi_m(\vec{\rho}_2, t_2) \\
&= \sum_{m \neq n} \int d\mathbf{k} \int d\mathbf{k}' |\alpha_m|^2 |\alpha_n|^2 [g_m^*(\mathbf{k}; \vec{\rho}_1, t_1) g_n(\mathbf{k}'; \vec{\rho}_1, t_1)] \\
&\quad [g_n^*(\mathbf{k}'; \vec{\rho}_2, t_2) g_m(\mathbf{k}; \vec{\rho}_2, t_2)] \\
&\propto \sum_m e^{-i(\vec{\kappa}_m \cdot (\vec{\rho}_1 - \vec{\rho}_2)/\mu + \phi(|\vec{\rho}_1 - \vec{\rho}_o|) - \phi(|\vec{\rho}_2 - \vec{\rho}_o'|))} \\
&\quad \sum_n e^{i(\vec{\kappa}_n \cdot (\vec{\rho}_1 - \vec{\rho}_2)/\mu + \phi(|\vec{\rho}_1 - \vec{\rho}_o|) - \phi(|\vec{\rho}_2 - \vec{\rho}_o'|))} \\
&\propto \text{somb}^2\left(\frac{\pi \Delta \theta_s}{\lambda} |\vec{\rho}_1 - \vec{\rho}_2|/\mu\right), \tag{9}
\end{aligned}$$

where we have assumed constant α of the subfields. Taking the small size of the lens into account, we have also assumed constant phase delays from $\vec{\rho}_o$ to $\vec{\rho}_1$ and $\vec{\rho}_2$ to simulate the behavior of a small lens that is unable to introduce large enough phase delays between different optical paths from $\vec{\rho}_o$ to $\vec{\rho}'_1 \neq \vec{\rho}_1$ and $\vec{\rho}'_2 \neq \vec{\rho}_2$. Referring to the earlier constructive-destructive interference picture of imaging, a constant phase delay indicates an “extremely poor” resolution.

Now, we calculate the integral of $\vec{\rho}_2$, i.e., the convolution between the object aperture $A(\vec{\rho}_o)$ and the intensity

fluctuation correlation:

$$\begin{aligned}
R_c(\vec{\rho}_1) &\simeq R_0 A^2(\vec{\rho}_2/(\mu)) \otimes \text{somb}^2\left(\frac{\pi \Delta \theta_s}{\lambda} |\vec{\rho}_1 - \vec{\rho}_2|/\mu\right) \\
&\simeq R_0 A^2(\vec{\rho}_1/(\mu)) \tag{10}
\end{aligned}$$

where the integral over $\vec{\rho}_2$ has been approximated as a δ function by assuming a large enough source. For smaller sources the imaging resolution is limited by the angular diameter $\Delta \theta_s$ of the source.

Referring to Eq. 7 we can see that the interference cross term corresponds to the photon-number fluctuation correlation. When $\vec{\rho}_1 = \vec{\rho}_2$, the two superposition terms $\psi_m(\vec{\rho}_1, t_1) \psi_n(\vec{\rho}_2, t_2) + \psi_m(\vec{\rho}_2, t_2) \psi_n(\vec{\rho}_1, t_1)$ take the same optical paths and for all m and n the superposition terms are in phase and constructively interfere. In this case, the interference cross term takes its maximum value and results in a maximum photon-number fluctuation correlation. However, when $\vec{\rho}_1 \neq \vec{\rho}_2$, the two terms superpose with a nonzero relative phase that depends on the transverse positions of the m th and n th sub-sources.

For a large angular diameter source, when $\vec{\rho}_1$ is slightly different from $\vec{\rho}_2$, the relative phases for different m - n pairs may take all possible values from zero to 2π , resulting in complete destructive addition for all m - n pairs when $\vec{\rho}_1 \neq \vec{\rho}_2$. In this case, the cross interference terms can be treated as a δ -function of $|\vec{\rho}_1 - \vec{\rho}_2|$. Then the maximum photon-number fluctuation correlation only occurs at $\vec{\rho}_1 = \vec{\rho}_2$, resulting in a perfect image reproduced in the photon-number fluctuation coincidences.

For a smaller angular source, when $\vec{\rho}_1$ is slightly different from $\vec{\rho}_2$, the maximum phase differences may not be able to reach 2π , resulting in an incomplete destructive addition of the superposition terms. In this case, the cross interference term $\text{somb}^2(\frac{\pi \Delta \theta_s}{\lambda} |\vec{\rho}_1 - \vec{\rho}_2|/\mu)$ cannot be treated as a δ -function. The photon-number fluctuation correlation function then has an increased width dependent on the angular size of the source $\Delta \theta_s$, resulting in limited imaging resolution. This second-order constructive-destructive interference determines its imaging resolution. It is interesting that while the observed image in photon-number fluctuation correlation is produced by constructive second-order interference, its resolution is limited by destructive second-order interference.

In summary, we have demonstrated the working principle of an imaging mechanism with nonclassical imaging resolution. The experimental result shows that even when the first-order classical images are “blurred” out due to the limited size of the imaging lens, this imaging mechanism can still completely resolve the object.

The authors wish to thank J. Simon and Hui Chen for their helpful discussions. This research was partially supported by NSF and the MII program.

-
- [1] E. Hecht, *Optics* (Addison Wesley, 2002).
- [2] J.-E. Oh, Y.-W. Cho, G. Scarcelli, and Y.-H. Kim, *Opt. Lett.* **38**, 682 (2013).
- [3] In Ref. [2], the authors provided a good summary for different types of second-order imaging. Some of their references, such as:
1. R. S. Bennink, S. J. Bentley, and R. W. Boyd, *Phys. Rev. Lett.* **89**, 113601 (2002).
 2. V. Giovannetti, S. Lloyd, L. Maccone, and J. H. Shapiro, *Phys. Rev. A* **79**, 013827 (2009).
 3. F. Guerrieri, L. Maccone, F. N. C. Wong, J. H. Shapiro, S. Tisa, and F. Zappa, *Phys. Rev. Lett.* **105**, 163602 (2010).
 4. C. Zhao, W. Gong, M. Chen, E. Li, H. Wang, W. Xu, and S. Han, *App. Phys. Lett.* **101**, 141123 (2012), 10.1063/1.4757874.
 5. X. H. Chen, I. N. Agafonov, K.-H. Luo, Q. Liu, R. Xian, M. V. Chekhova, and L.-A. Wu, *Opt. Lett.* **35**, 1166 (2010).
 6. P. Zhang, W. Gong, X. Shen, D. Huang, and S. Han, *Opt. Lett.* **34**, 1222 (2009).
 7. G. Brida, M. V. Chekhova, G. A. Fornaro, M. Genovese, E. D. Lopaeva, and I. R. Berchera, *Phys. Rev. A* **83**, 063807 (2011).
 8. S. Mouradian, F. N. C. Wong, and J. H. Shapiro, *Opt. Exp.* **19**, 5480 (2011).
- belong to group one. The imaging resolution of group one is limited by the size of the imaging lens or other mechanisms that limit the ability to achieve first-order constructive-destructive interferences.
- The following references are in group two. The imaging resolution of group two is limited by the size of light source or other mechanisms that limit the ability to achieve second-order constructive-destructive interferences.
1. Ref. [7]
 2. R. E. Meyers, K. S. Deacon, and Y. Shih, *Phys. Rev. A* **77**, 041801 (2008).
 3. R. E. Meyers, K. S. Deacon, and Y. Shih, *Appl. Phys. Lett.* **98**, 111115 (2011).
 4. R. E. Meyers, K. S. Deacon, and Y. Shih, *Appl. Phys. Lett.* **100**, 131114 (2012).
 - [4] Note, the convolution of Eq.(2) and the autocorrelation of two identical classical images are different mathematically and physically.
 - [5] J. Cheng, *Opt. Express* **17**, 7916 (2009).
 - [6] R. Meyers, K. Deacon, and Y. Shih, *Journal of Modern Optics* **54**, 2381 (2007), <http://dx.doi.org/10.1080/09500340701400117>.
 - [7] A. Valencia, G. Scarcelli, M. D'Angelo, and Y. Shih, *Phys. Rev. Lett.* **94**, 063601 (2005).
 - [8] H. Chen, T. Peng, and Y. Shih, *Phys. Rev. A* **88**, 023808 (2013).
 - [9] T. Peng, H. Chen, Y. Shih, and M. O. Scully, *Phys. Rev. Lett.* **112**, 180401 (2014).
 - [10] H. Chen, *The high-order quantum coherence of thermal light*, Ph.D. thesis, University of Maryland Baltimore County (2014).
 - [11] R. J. Glauber, *Phys. Rev.* **131**, 2766 (1963).
 - [12] Y. Shih, *An Introduction to Quantum Optics: Photon and Biphoton Physics* (Taylor & Francis, 2011).
 - [13] M. O. Scully and M. S. Zubairy, *Quantum Optics* (Cambridge University Press, 1997).